Journal of Magnetism and Magnetic Materials 518 (2021) 167377

Contents lists available at ScienceDirect

Journal of Magnetism and Magnetic Materials

journal homepage: www.elsevier.com/locate/jmmm

Research articles

Spin wave modes of nanoellipses with a magnetic radial vortex configuration

H. Vigo-Cotrina[a,*], A.P. Guimarães[a]

[a] Centro Brasileiro de Pesquisas Físicas, 22290-180 Rio de Janeiro, RJ, Brazil

ARTICLE INFO

Keywords:
Radial magnetic vortex
Spin wave modes
Nanoellipse
Micromagnetic simulation

ABSTRACT

Radial vortices are exotic magnetic configurations that have several potential applications in Spintronics. In this paper, using micromagnetic simulation, we have proved that magnetic radial vortices can also be found in elliptic nanostructures, and have obtained the frequencies of their spin wave modes as a function of the sizes and ellipticity of the structures (here, we have defined the ellipticity as the ratio of the major axis to the minor axis $D = D_x/D_y$). Our results show that the size of the core of the magnetic radial vortex is not dependent on D. We have also obtained the spatial distribution of Fourier transform power spectra of the spin wave modes. Our results show that the variation in the values of D leads to the emergence of new spin wave modes, and that in general, the increase in the values of D leads to a decrease in the values of the frequencies of the spin wave modes.

1. Introduction

Magnetic vortices are exotic magnetic configurations that may be present in circular and elliptical nanostructures [1–6]. Up to now there are two types of magnetic vortices that are studied in the literature: circular vortices [1–8] and radial vortices [3,9–17].

Circular vortices are characterized by having a curling in-plane magnetization, and an out-of-plane magnetization in their cores [2,18]. The curling direction of the magnetization defines the circulation C. $C = +1$ when the curling direction is counterclockwise (CCW), and $C = -1$ when it is clockwise (CW). The region where occurs the out-of-plane component is called the vortex core; the direction of this component defines the polarity p of the vortex. If $p = +1$, the out-of-plane component points along the $+z$ direction, and if $p = -1$, along the -z direction [2,18]. Accordingly, there are four degenerate states for magnetic vortices (all combinations of C and p) [3,19,20].

Circular vortices in nanostructures have been the object of a large number of studies due to their several potential applications in Spintronics [21–23] and Medicine [24–26]. Circular vortices also allow the simulation of phenomena that are present in different areas of physics [7,8,27,28].

The magnetic radial vortex configuration has attracted interest in recent years [3,9–17]. It also has an in-plane component and an out-of-plane component of the magnetization, but unlike the circular magnetic vortex, the profile of the in-plane components of the magnetization point in a radial (i.e., towards the center), or antiradial (away from the center) direction [3]. Another important difference is that these vortices have only two degenerate states, e.g., if $p = +1$, the in-plane components point in the radial direction, and if $p = -1$, the in-plane components point in the antiradial direction [3].

Radial vortices in circular nanostructures have been obtained by micromagnetic simulations [3,9–11,13–17], and have been observed experimentally [12].

In an analogous way to circular vortices, the dynamics of the radial vortices can be induced by the application of an external perturbation, e.g., a spin polarized current [14], or a magnetic field pulse [3]. The issue of the switching of the radial vortex core is a subject of study in the literature. The core of a radial vortex can be switched using either of these perturbations; spin polarized current [9,15,29], or magnetic fields [10,11,16]. The efficiency of the switching process, using magnetic fields, depends of the right choice of the frequency of the spin wave mode to be used. For this, it is necessary to know the distribution of the spin wave modes in the nanostructure. The study of the frequencies and spatial distribution of spin wave modes was recently performed using magnetic radial vortices and skyrmioniums [11,30], a prerequisite for Spintronic applications of the switching of these exotic magnetic structures.

Although there is a growing interest in the study of magnetic radial vortices, the issue of the stabilization and of the frequencies of the spin wave modes in this type of magnetic configurations in elliptical

* Corresponding author.
E-mail address: vigohel@outlook.com (H. Vigo-Cotrina).

https://doi.org/10.1016/j.jmmm.2020.167377
Received 16 April 2020; Received in revised form 8 July 2020; Accepted 31 August 2020
Available online 14 September 2020
0304-8853/

nanostructures remains unexplored. For this reason, we have studied how the size and the shape of the nanostructure influence these modes. We have used the GPU-accelerated micromagnetic simulation program MuMax3 [31], with a cell size $2 \times 2 \times L\ nm^3$, where L is the thickness of the ferromagnetic layer. The typical parameters of Permalloy used were [2,9,14]: saturation magnetization $M_s = 8{\times}10^5$ A/m, exchange stiffness constant $A_{ex} = 1.3{\times}10^{-11}$J/m, damping constant $\alpha = 0.01$ and negligible crystalline anisotropy.

2. Results and discussion

We have simulated a $D_x \times D_y \times L$ Permalloy elliptical ferromagnetic (FM) layer, where D_x is the length of the major axis (along the x axis) of the nanostructure, D_y is the length of the minor axis (along the y axis) and L = 1 nm is the thickness. The FM layer is coupled to a non-magnetic layer (NM). The coupling between FM and NM layers leads to a negative Dzyaloshinskii-Moriya exchange constant $D_{int} = -2.3$ mJ/m [9,14]. We kept a fixed value of $D_y = 200$ nm, and defined the ratio $D = D_x/D_y$.

In order to obtain the ground state of the nanostructure, we have considered in our micromagnetic simulations two initial magnetic configurations: circular vortex, and radial vortex. We have obtained as final magnetic configuration, radial magnetic vortices with polarity p = +1 and in-plane components pointing away from the center, for all our values of D[1], ranging between D = 1, and D = 2. The z-component of the magnetization of the radial vortex is shown in the color code in Fig. 1 (a), for several values of D. The profile of the z-component of the magnetization m_z along the major axis of the ellipse is shown in Fig. 1 (b).

In all cases, the diameters of the core of the radial vortices have almost the same value[2], of approximately 25.7, nm. These values were measured both along the major axis and along the minor axis (only the values of m_z along x appear in Fig. 1 (b)). This agreement, for all values of D used in this study, is shown in Fig. 1 (b) for m_z computed along the major axis.

In order to obtain the frequencies of the spin wave modes, we started our simulations with the magnetic radial vortex configuration as the initial state in the nanoellipse. Next, we have applied a perpendicular sinc magnetic field pulse $B_z = B_0 Sinc(2\pi f(t\text{-}t_0))$, where $B_0 = 20$ mT and $t_0 = 1$ ns. In this stage, we used a lower damping constant, $\alpha = 0.005$, for better resolution of the spin wave modes. The average z-component $\langle m_z(t)\rangle$ of the magnetization was saved every 5 ps for a total of 20, ns. The same procedure was repeated for all our values of the ellipticity D.

The power spectra were obtained by a fast Fourier transform (FFT) of the temporal evolution of the fluctuations of the z-component $\delta m_z = \langle m_z(t)\rangle - \langle m_z(t = 0)\rangle$ of the magnetization of the whole nanostructure (see Ref. [33] for details), where $\langle m_z(t)\rangle$ was obtained in the previous step. The power spectra for several values of D are shown in Fig. 2.

We have started by describing the case for D = 1, since this will be used to compare with the cases $D \neq 1$. In Fig. 2 (a) it is shown the power spectrum for D = 1 (circular nanostructure). In this figure, we can see five prominent peaks at approximately $f_1 = 4.41$ GHz (mode 1), $f_2 = 8.68$ GHz (mode 2), $f_3 = 13.59$ GHz (mode 3), $f_4 = 19.99$ GHz (mode 4) and $f_5 = 37.23$ GHz (mode 6)[3].

The spatial distribution of FFT power of the spin wave modes is shown in Fig. 3 (a-e), for D = 1. From this figure, we can see that, for mode 1, the maximum oscillation amplitudes are located around the center, both along the x-axis and the y axis (Fig. 3 (a)). For mode 2, the maximum oscillation amplitudes are also located around the center, both along the x-axis and the y axis (Fig. 3 (b)). However, for this mode, the area of the region of maximum amplitude is smaller compared to that of mode 1. Additionally, for mode 2, there are also maximum oscillation amplitudes at the edges (Fig. 3 (b)).

For modes 3, 4, and 6 (Fig. 3 (c-e)), the maximum oscillation amplitude is located in such a way that it forms a ring around the center and occupies a smaller region, compared to those of modes 1 and 2.

From Figs. 3 (a-e) it is possible to determine that mode 1, mode 2, mode 3, mode 4 and mode 6 have one, two, three, four and six nodes, respectively, in the radial direction (see Supplementary Material to see the profile of the FFT power along the nanodisk).

In order to obtain more information on the dynamics of the modes, we have applied an alternating perpendicular magnetic field pulse $B_z = B\sin(2\pi ft)$, where f is the frequency of the spin wave mode, B = 0.5 mT and t is the time of duration (t = 2 ns). During the application of this magnetic field, the spatial fluctuations $\delta m_z = (m_z(t) - m_z(t = 0))$ are calculated. The snapshots of the spatial distribution of these fluctuations are shown in Fig. 3 (f-j) for each mode. In these figures, we can see that the spatial distributions of δm_z have shapes similar to the spatial distribution of FFT power shown in Fig. 3 (a-e). The dynamics[4] of the fluctuations δm_z shown in Fig. 3 (f-j) allows us to know more details about the modes: in this case, all modes shown in Fig. 3 oscillate in the z-direction.

For D = 1, these modes are like those obtained for the circular vortex, i.e., concentrated around the vortex core and oscillating in the z-direction (standing spin waves), as already shown by Yoo et *al.* [34], and Wang et *al.* [35]. It is important to note here that in our case, the presence of D_{int} leads to a non-symmetric propagation of the spin wave (see Ref. [36] for more details). Thus, the expression "standing spin wave" is not appropriate to be applied in our case.

For D = 1.2, the frequencies of the spin wave modes mentioned above, change their values and new modes appear. This behavior can be seen in Fig. 2 (b). The frequency of mode 1 decreases to approximately 4.05GHz, for mode 2 to 7.68 GHz, for mode 3 to 12.14 GHz, for mode 5 to 33.27 GHz, and mode 4 vanishes. Additionally, it is possible to observe the appearance of new peaks in the frequency spectrum (Fig. 2 (b)). This is expected, since the origin of radial modes in magnetic nanostructures is due to the dipolar interaction [32,37]; thus, for $D \neq 1$ (and fixed D_y), there is an increase in the dipolar energy due to the increase of the size of the nanostructure. This increase is responsible for the emergence of new modes [32]. The new peaks represent new frequencies of spin wave modes in the nanostructure. There are a total number of 7 peaks for D = 1.2.

The spatial distributions of FFT power of the spin wave modes and the snapshots of the fluctuations δm_z for D = 1.2 are shown in Fig. 4 (a-g) and Fig. 4 (h-n), respectively. The spatial distributions of FFT power of the modes are different from those shown in Fig. 3. For example, for mode 1, the maximum oscillation amplitudes are distributed principally around the center, slightly tilted from the y-axis (Fig. 4 (a)). Additionally, there are small oscillations, both surrounding the maximum oscillations and on the edges. For mode 2, there are maximum oscillation amplitudes around the center, but they deviate significantly from both the x-axis and y-axis (Fig. 4 (b)). This mode has also small oscillations surrounding the maximum oscillations, but smaller in amplitude compared to mode 1. For mode 3, the maximum oscillation amplitudes are distributed mostly around the center, slightly tilted from the y-axis

[1] In our micromagnetic simulations, we have assumed temperature T = 0. However, in the Supplementary Material we show that it is possible to obtain radial vortices at room temperature (T = 300, K).

[2] This behavior is different from that found for other magnetic configurations, e.g., Liu et al. [32] have shown that the size of the core of a skyrmion increases with the increase of D.

[3] This is mode 6, because the system has in general 6 nodes, as will be mentioned later.

[4] Note that the snapshots of δm_z shown along the present paper are for an instant of time t. The temporal evolution of δm_z allows the observation of the character of the mode, that is, if it corresponds only to an oscillation δm_z, or if the distribution of δm_z also rotates. See video in the Supplementary Material.

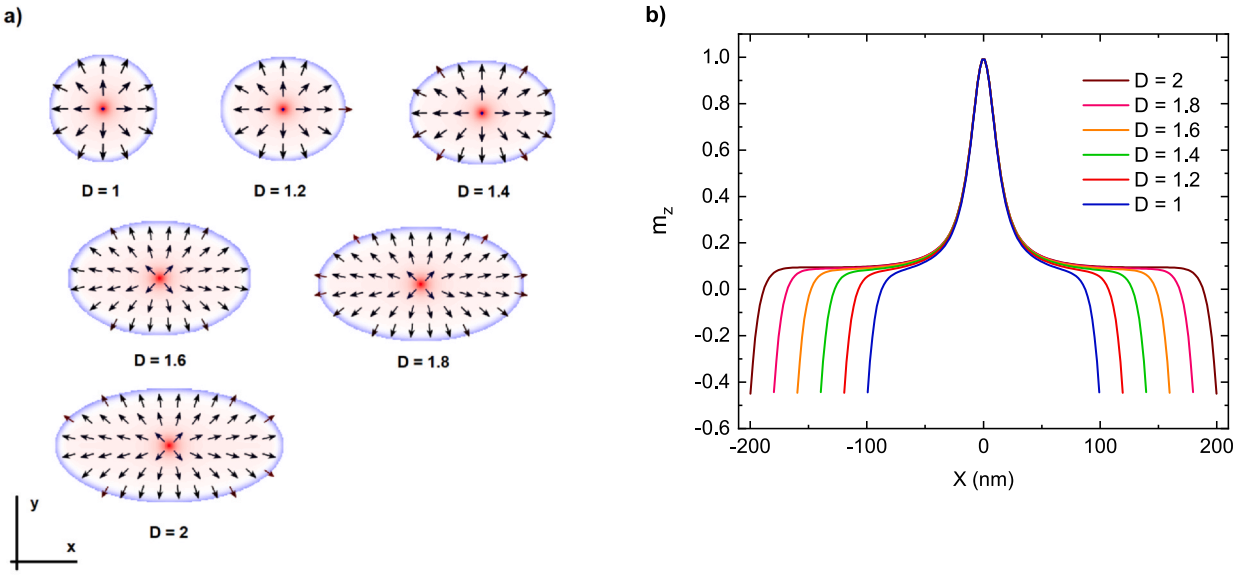

Fig. 1. (a) Images of the spatial z-component of the magnetization in the FM layer for several values of D, and (b) profiles of the z-component of the magnetization along the x direction, for different values of D.

(Fig. 4 (c)), in a similar way to mode 1, but the region of maximum amplitude is smaller than the one shown in Fig. 4 (a). Mode 4 has the maximum oscillation amplitudes distributed mostly around the center, slightly tilted from the x-axis (Fig. 4 (d)) and small oscillation around the center, along y-axis and at the edges. Mode 5 ((Fig. 4 (e))) and mode 6 (Fig. 4 (f)) have the maximum oscillation amplitudes distributed mostly around the center, slightly tilted from the y-axis and x-axis, respectively. Additionally, these modes present small oscillations at the edges. Mode 7 has the maximum oscillation amplitudes distributed mostly in spots around the center and at the edges (Fig. 4 (g)). This mode is different from the modes mentioned above.

Additionally, analyzing the dynamics of the fluctuation δm_z (Fig. 4 (h-n)), we observed that the new mode 1 (f = 4.05 GHz) shown in Fig. 4 (h), rotates in the clockwise direction around the center and oscillates in the z-direction. This is different from mode 1 shown in Fig. 3 (a), where there is only oscillation in the z-direction. Mode 2 (Fig. 4 (i)), mode 3 (Fig. 4 (j)), mode 4 (Fig. 4 (k)), mode 5 (Fig. 4 (l)), mode 6 (Fig. 4 (m)), and mode 7 (Fig. 4 (n)) are also a mixture of rotating mode in the clockwise direction and oscillating mode.

It is important to note here that the change of the shape of the magnetic nanostructure modifies drastically the spatial profile of the spin wave modes and their dynamic characteristics.

For D = 1.4, the frequencies of the spin wave modes decrease their values. This behavior can be seen in Fig. 2 (c). There is also the appearance of new peaks in the power spectrum. For example, a lower frequency appears (f = 1.77 GHz).

In order to compare these new modes with those of the case D = 1.2, we show only the mode corresponding to the more intense peaks. The spatial distribution of FFT power of the spin wave modes and the snapshots of the fluctuations δm_z are shown in Fig. 5 (a-d) and Fig. 5 (e-h), respectively. For the lowest frequency mode (Fig. 5 (a)) the maximum oscillation amplitudes are distributed mostly around the center, slightly tilted from the x-axis. There are small amplitudes at the edges. For mode 2 (Fig. 5 (b)), the maximum oscillation amplitudes are distributed in a similar way as mode 1 shown in Fig. 4 (a), but the region of maximum amplitude is smaller than the one shown in Fig. 4 (a). Note that the variation of ellipticity D, from D = 1.2 to D = 1.4, modified only the size of the region of maximum amplitude in each of the modes, however, both modes keep the same shape of the distribution of maximum oscillation amplitudes.

Mode 3 (Fig. 5 (c)) has the maximum oscillation amplitudes distributed around the center, slightly tilted from the x-axis, and a small oscillation at the edges. This distribution of maximum oscillation amplitudes contrasts with the corresponding distribution for mode 2 shown in Fig. 4 (b). In this case, the variation of ellipticity D, from D = 1.2 to D = 1.4, modifies the distribution of the maximum oscillation amplitude. For mode 4 (Fig. 5 (d)), the maximum oscillation amplitudes are distributed around the center, and at the edges in the form of spots. This distribution of the maximum oscillation amplitudes contrasts with the distribution of mode 3 shown in Fig. 4 (c). For the other modes of higher frequency (not shown here), the distributions of the maximum oscillation amplitudes also change and are not similar to those modes shown in Fig. 4 (d-g).

Analyzing the dynamics of the fluctuations δm_z (Fig. 5 (e-h)), we have that all modes mentioned above are a mixture of rotating mode in the clockwise direction and oscillation mode.

For D = 1.6 and D = 1.8, the number of prominent peaks increases to eleven, and for D = 2, to twelve peaks (see Fig. 2 (d-f)). The shape of the distribution of the maximum oscillation amplitudes is the same for some modes and different for others. For example, mode 1 shown in Fig. 5 (a) has the same shape of the distribution of the maximum oscillation amplitudes for D = 1.6 and D = 1.8. However, the size of the region of maximum oscillation amplitudes increases with the increase of D, and for D = 2, the shape of the distribution of the maximum oscillation amplitudes is different from the cases for D = 1.4 and D = 1.6. A similar behavior is found for mode 3 (Fig. 5 (c)). Other modes shown in Fig. 2 (d-f) have different distributions of maximum amplitude of oscillation for each value of frequency.

Note that the modes for D ≠ 1 are different from the azimuthal modes of circular vortices, which come in pairs (one of them rotates in the clockwise direction and the other in the counterclockwise direction) [38,39].

Similar behaviors in the dynamics of spin wave modes in nanoellipses were obtained for a skyrmion [32].

Additionally, we have performed simulations (not shown here) considering p = −1 (thus, anti-radial direction). Our results show that the mode rotations as a function of time have clockwise sense for p = +1 and counterclockwise for p = -1. Also, we have considered the case

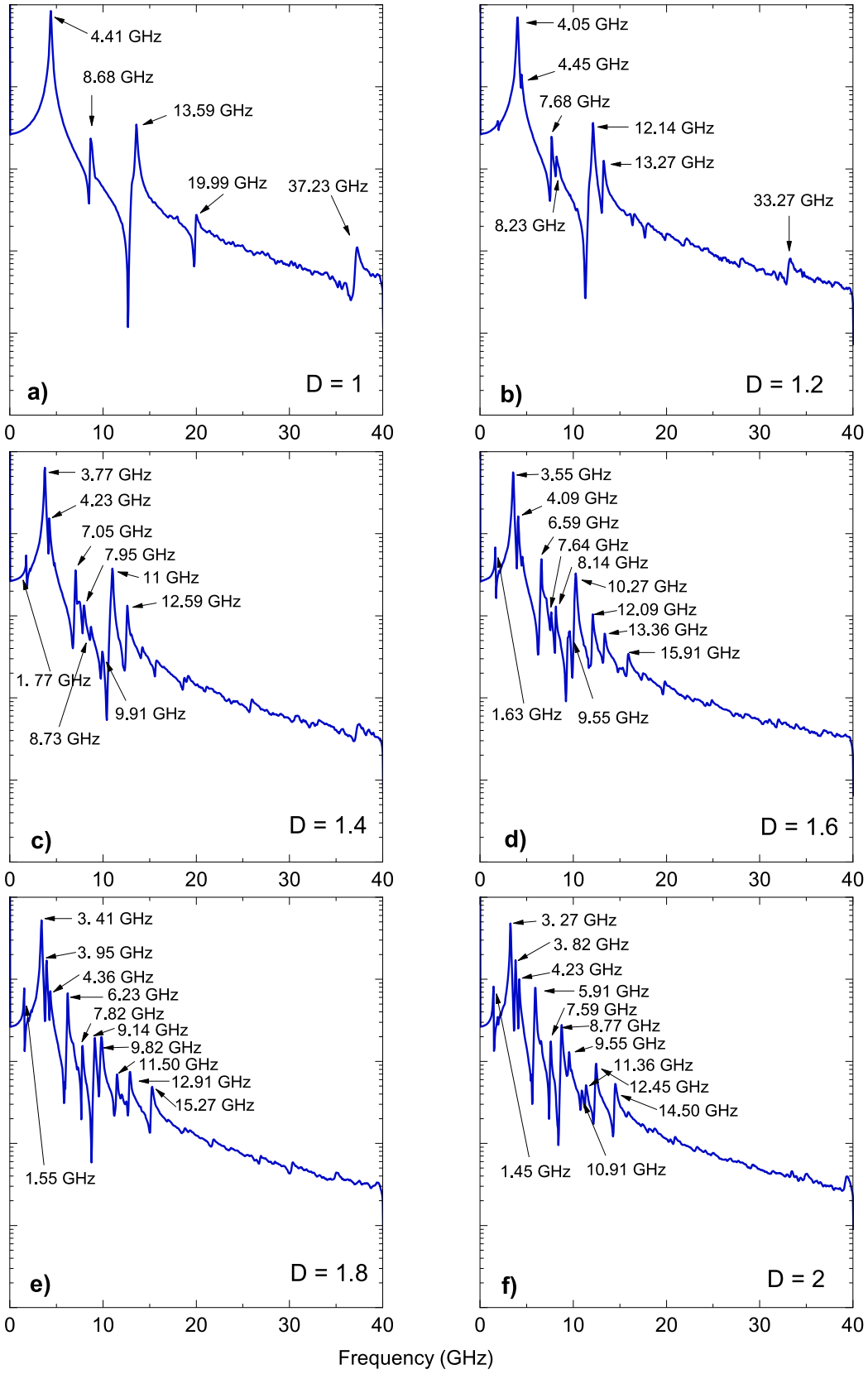

Fig. 2. Power spectra obtained by fast Fourier transform for several values of ellipticity D.

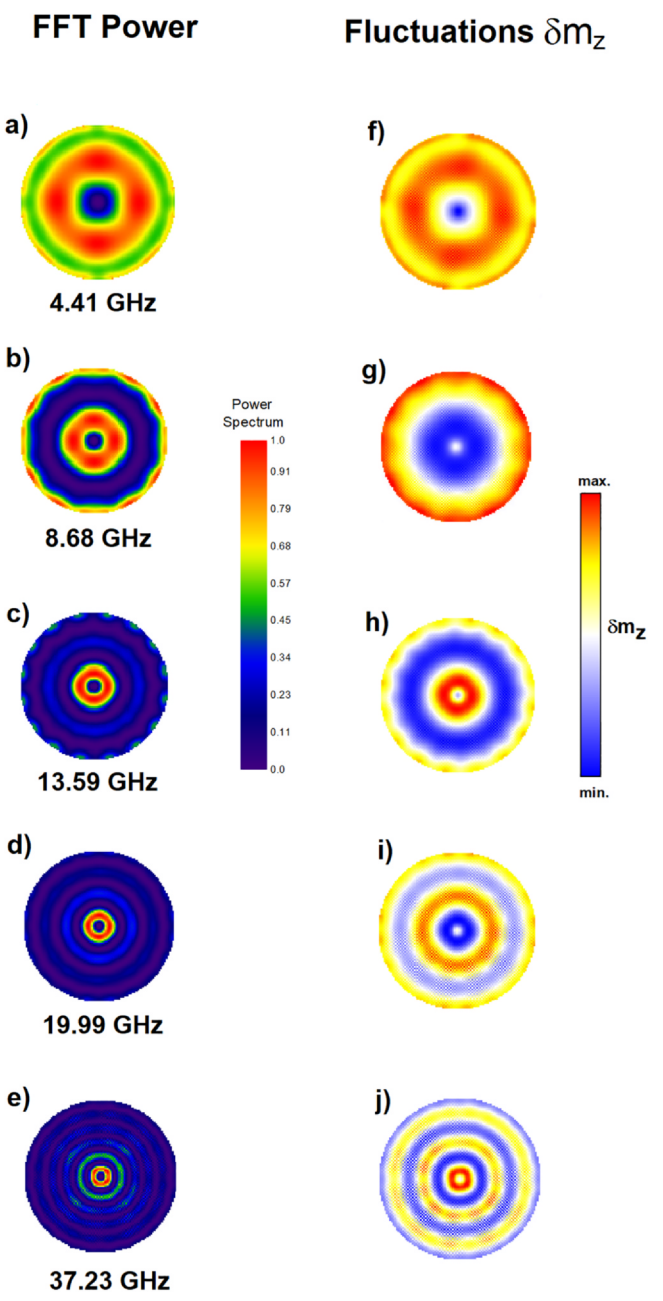

Fig. 3. (a-e) show the spatial distribution of Fourier power of the spin wave modes for D = 1, and (f-j) show the dynamics of the spatial fluctuations $\delta m_z = < m_z(t) > - < m_z(t = 0) >$.

for $D_{int} > 0$. The results show that the sense of rotation does not depend on the sign of D_{int}, only on the polarity p.

3. Conclusions

In summary, in this work, we have demonstrated the formation of radial vortices in Permalloy elliptic nanostructures coupled to a non-magnetic layer, using micromagnetic simulation. Our results show that it is possible to obtain radial vortices in elliptic nanostructures for several different ellipticities D. We have also shown that the values of the frequencies of the power spectrum and the spatial distributions of the FFT power is dependent on the value of D. Our results show that the dynamics of the modes depends on the values of D. In the case of circular geometry (D = 1), the modes oscillate in the z-direction, but the increase in the values of D leads to complex modes that are

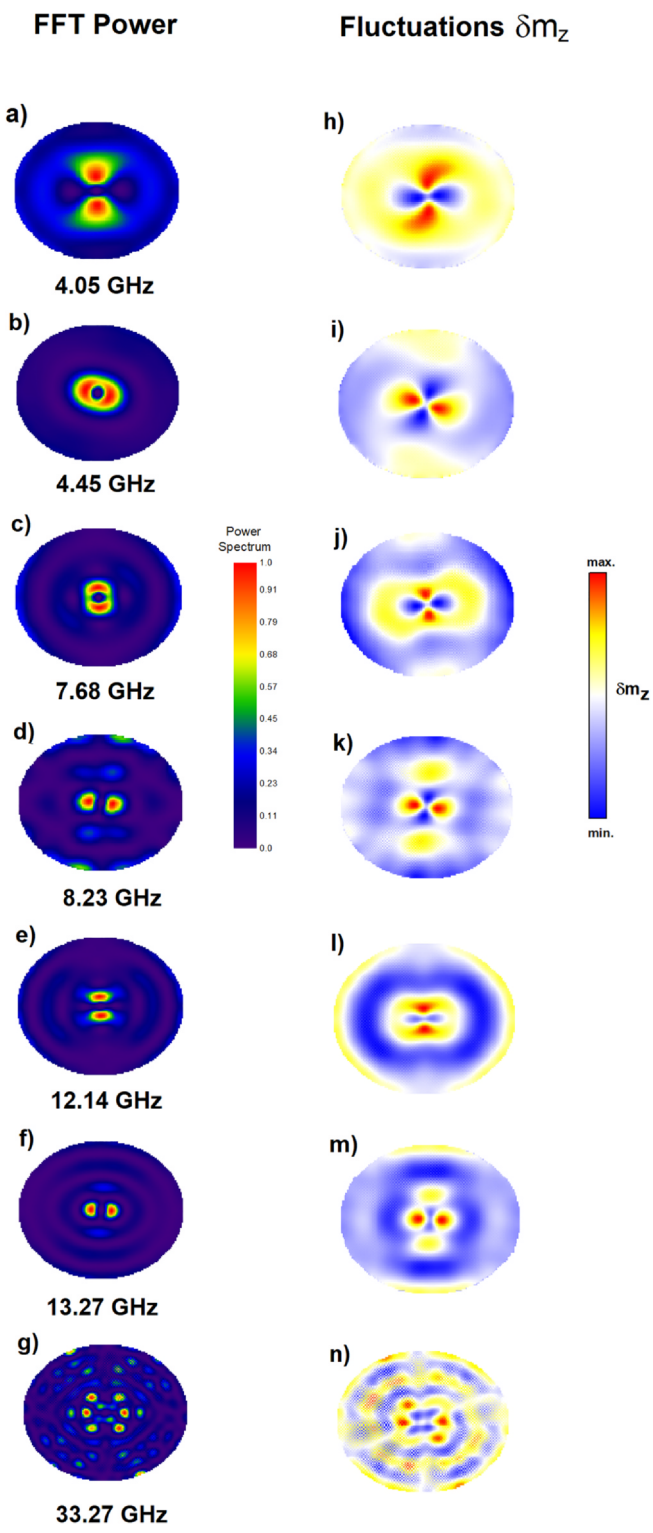

Fig. 4. (a-g) show the spatial distribution of Fourier power of the spin wave modes for D = 1.2, and (h-n) show the dynamics of the spatial fluctuations $\delta m_z = < m_z(t) > - < m_z(t = 0) >$.

combinations of rotating and oscillating modes.

These results are relevant, since they show the complexity of the shape and dynamics of the spin wave modes in nanoellipses with magnetic radial vortex configuration, which can be used, for example, to perform the switching of the vortex cores. In an eventual application of radial vortex structures, a precondition for the choice of more effective switching parameters is the knowledge of how these modes are

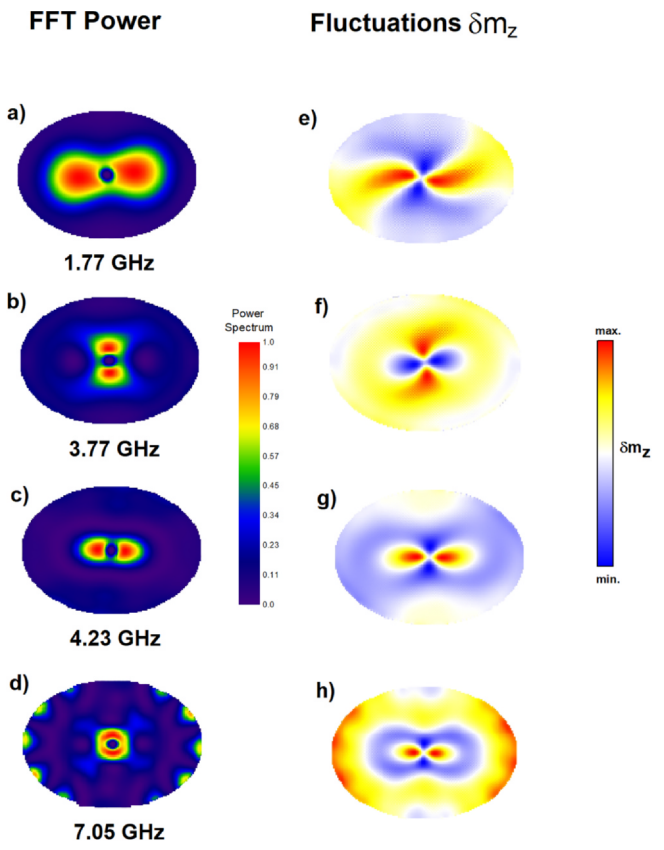

Fig. 5. (a-d) show the spatial distribution of Fourier power of the spin wave modes for D = 1.4, and (e-h) show the dynamics of the spatial fluctuations $\delta m_z = < m_z(t) > - < m_z(t = 0) >$.

distributed in the nanostructure.

Credit authorship contribution statement

H. Vigo-Cotrina: Conceptualization, Methodology, Software, Writing - original draft. **A.P. Guimarães:** Supervision, Writing - review & editing, Resources.

Declaration of Competing Interest

The authors declare that they have no known competing financial interests or personal relationships that could have appeared to influence the work reported in this paper.

Acknowledgments

The authors would like to thank the support of the Brazilian agencies FAPERJ and CNPq.

Appendix A. Supplementary data

Supplementary data associated with this article can be found, in the online version, at https://doi.org/10.1016/j.jmmm.2020.167377.

References

[1] H. Li, D. Li, Y. Wang, Z. Hua, The magnetic vortex gyration mediated by spin-polarized current in a confined off-centered nanocontact structure, Solid State Commun. 251 (2017) 60–65, https://doi.org/10.1016/j.ssc.2016.12.015.
[2] A.P. Guimarães, Principles of Nanomagnetism, 2nd Edition, Springer, Cham, 2017.
[3] G. Siracusano, R. Tomasello, A. Giordano, V. Puliafito, B. Azzerboni, O. Ozatay, M. Carpentieri, G. Finocchio, Magnetic radial vortex stabilization and efficient manipulation driven by the Dzyaloshinskii-Moriya interaction and spin-transfer torque, Phys. Rev. Lett. 117 (2016) 087204, , https://doi.org/10.1103/PhysRevLett.117.087204.
[4] C. Zaspel, Vortex precession in thin elliptical ferromagnetic nanodisks, J. Magn. Magn. Mater. 433 (2017) 59–63, https://doi.org/10.1016/j.jmmm.2017.02.044.
[5] H. Hata, M. Goto, A. Yamaguchi, T. Sato, Y. Nakatani, Y. Nozaki, Coupled oscillations of vortex cores confined in a ferromagnetic elliptical disk, Phys. Rev. B 90 (2014) 104418, , https://doi.org/10.1103/PhysRevB.90.104418.
[6] C.F. Gélvez, E.J. Patiño, Coercive field enhancement in co nanodisks: single-domain to vortex switching, J. Phys.: Condens. Matter 31 (13) (2019) 13LT01, https://doi.org/10.1088/1361-648x/ab015e.
[7] C. Zaspel, Synchronization of vortex-based spin torque nano-oscillators by magnetostatic coupling, J. Magn. Magn. Mater. 396 (2015) 172–175, https://doi.org/10.1016/j.jmmm.2015.08.027.
[8] F. Abreu Araujo, J. Grollier, Controlling the synchronization properties of two dipolarly coupled vortex based spin-torque nano-oscillators by the intermediate of a third one, J. Appl. Phys. 120 (10) (2016) 103903, , https://doi.org/10.1063/1.4962014.
[9] Y. Ma, R. Zhao, C. Song, C. Jin, J. Wang, Y. Wei, Y. Huang, J. Wang, J. Wang, Q. Liu, Current-driven radial vortex switching in a permalloy nanodisk, J. Magn. Magn. Mater. 491 (2019) 165544, , https://doi.org/10.1016/j.jmmm.2019.165544.
[10] C. Li, L. Fang, X. Yang, N. Xu, B. Liu, B. Wei, E. Zhou, B. Yang, In situ control of radial vortex polarity at room temperature utilizing perpendicular magnetic field pulse, J. Phys. D: Appl. Phys. 53 (1) (2019) 015001, , https://doi.org/10.1088/1361-6463/ab4837.
[11] Y. Ma, C. Song, C. Jin, J. Wang, H. Xia, Y. Wei, J. Wang, Q. Liu, Microwave-driven dynamic switching of the radial vortex in a nanodot by micromagnetic simulation, J. Phys. D: Appl. Phys. 52 (19) (2019) 195001, , https://doi.org/10.1088/1361-6463/ab0356.
[12] I. Cinar, C. Yanik, R. Tomasello, S. Tacchi, G. Siracusano, M. Carpentieri, G. Finocchio, T. Hauet, O. Ozatay, Observation of magnetic radial vortex nucleation in a multilayer stack with tunable anisotropy, Sci. Rep. 8 (2018) 7180, https://doi.org/10.1038/s41598-018-25392-x.
[13] R.V. Verba, D. Navas, A. Hierro-Rodriguez, S.A. Bunyaev, B.A. Ivanov, K.Y. Guslienko, G.N. Kakazei, Overcoming the limits of vortex formation in magnetic nanodots by coupling to antidot matrix, Phys. Rev. Appl. 10 (2018) 031002, , https://doi.org/10.1103/PhysRevApplied.10.031002.
[14] D. Dong, C. Li, L. Cai, B. Liu, C. Li, J. Liu, Y. Chen, Magnetic radial vortex core and coupled edge-soliton pair gyration dynamics, IEEE Magn. Lett. 10 (2019) 1–5, https://doi.org/10.1109/LMAG.2019.2925584.
[15] D. Dong, L. Cai, C. Li, B. Liu, C. Li, J. Liu, Radial vortex core reversal driven by a spin-polarized current in a nanocontact structure, J. Phys. D: Appl. Phys. 52 (29) (2019) 295001, , https://doi.org/10.1088/1361-6463/ab1c46.
[16] C. Li, L. Cai, X. Yang, H. Cui, S. Wang, B. Wei, D. Dong, C. Li, J. Liu, B. Liu, Subnanosecond radial vortex core polarity reversal using linearly attenuated perpendicular magnetic field, IEEE Magn. Lett. 9 (2018) 1–4, https://doi.org/10.1109/LMAG.2018.2806893.
[17] R.V. Verba, D. Navas, S.A. Bunyaev, A. Hierro-Rodriguez, K.Y. Guslienko, B.A. Ivanov, G.N. Kakazei, Helicity of magnetic vortices and skyrmions in soft ferromagnetic nanodots and films biased by stray radial fields, Phys. Rev. B 101 (2020) 064429, , https://doi.org/10.1103/PhysRevB.101.064429.
[18] K.Y. Guslienko, Low-frequency vortex dynamic susceptibility and relaxation in mesoscopic ferromagnetic dots, Appl. Phys. Lett. 89 (2) (2006) 022510, , https://doi.org/10.1063/1.2221904.
[19] D. Toscano, S.A. Leonel, R.A. Dias, P.Z. Coura, J.C.S. Rocha, B.V. Costa, Magnetic vortex formation and gyrotropic mode in nanodisks, J. Appl. Phys. 109 (1) (2011) 014301, , https://doi.org/10.1063/1.3526970.
[20] M.-Y. Im, P. Fischer, K. Yamada, T. Sato, S. Kasai, Y. Nakatani, T. Ono, Symmetry breaking in the formation of magnetic vortex states in a permalloy nanodisk, Nature Communications 3. doi:10.1038/ncomms1978.
[21] S. Bohlens, B. Krüger, A. Drews, M. Bolte, G. Meier, D. Pfannkuche, Current controlled random-access memory based on magnetic vortex handedness, Applied Physics Letters 93 (14). doi:10.1063/1.2998584.
[22] B. Pigeau, G. de Loubens, O. Klein, A. Riegler, F. Lochner, G. Schmidt, L.W. Molenkamp, V.S. Tiberkevich, A.N. Slavin, A frequency-controlled magnetic vortex memory, Applied Physics Letters 96 (13). doi:10.1063/1.3373833.
[23] H. Jung, Y.-S. Choi, K.-S. Lee, D.-S. Han, Y.-S. Yu, M.-Y. Im, P. Fischer, S.-K. Kim, Logic operations based on magnetic-vortex-state networks, ACS Nano 6 (5) (2012) 3712–3717, pMID: 22533663. doi:10.1021/nn3000143.
[24] Y. Yang, X. Liu, Y. Lv, T.S. Herng, X. Xu, W. Xia, T. Zhang, J. Fang, W. Xiao, J. Ding, Orientation mediated enhancement on magnetic hyperthermia of Fe3O4 nanodisc, Adv. Funct. Mater. 25 (5) (2015) 812–820, https://doi.org/10.1002/adfm.201402764.
[25] A. Dong-Hyun Kim, V. Rozhkova, D. Ulasov, T. Bader, S. Rajh, V. Novosad Lesniak, Biofunctionalized magnetic-vortex microdiscs for targeted cancer-cell destruction, Nature Mater. 9 (2010) 165–171, https://doi.org/10.1038/nmat2591.
[26] P. Tiberto, G. Barrera, F. Celegato, G. Conta, M. Coïsson, F. Vinai, F. Albertini, Ni80Fe20 nanodisks by nanosphere lithography for biomedical applications, J. Appl. Phys. 117 (17) (2015) 17B304, https://doi.org/10.1063/1.4913278.
[27] J.P. Sinnecker, H. Vigo-Cotrina, F. Garcia, E.R.P. Novais, A.P. Guimarães, Interaction between magnetic vortex cores in a pair of nonidentical nanodisks, J. Appl. Phys. 115 (2014) 203902, , https://doi.org/10.1063/1.4878875.
[28] H. Vigo-Cotrina, A.P. Guimarães, Parallels between a system of coupled magnetic vortices and a ferromagnetic/nonmagnetic (FM/NM) multilayer system, J. Magn. Magn. Mater. 497 (2020) 166009, , https://doi.org/10.1016/j.jmmm.2019.166009.

[29] C. Li, S. Wang, N. Xu, X. Yang, B. Liu, B. Yang, L. Fang, Spin-torque nano-oscillators based on radial vortex in the presence of interface Dzyaloshinskii-Moriya interaction, J. Magn. Magn. Mater. 498 (2020) 166155, , https://doi.org/10.1016/j.jmmm.2019.166155.

[30] H. Vigo-Cotrina, A.P. Guimarães, Switching of skyrmioniums induced by oscillating magnetic field pulses, J. Magn. Magn. Mater. 509 (2020) 166895, , https://doi.org/10.1016/j.jmmm.2020.166895.

[31] A. Vansteenkiste, J. Leliaert, M. Dvornik, M. Helsen, F. Garcia-Sanchez, B. Van Waeyenberge, The design and verification of Mumax3, AIP Adv. 4 (2014) 107133, , https://doi.org/10.1063/1.4899186.

[32] Y. Liu, R.K. Lake, J. Zang, Shape dependent resonant modes of skyrmions in magnetic nanodisks, Journal of Magnetism and Magnetic Materials 455 (2018) 9–13, magnetic skyrmions as future information carriers. doi: 10.1016/j.jmmm.2017.07.007.

[33] A. Baker, M. Beg, G. Ashton, M. Albert, D. Chernyshenko, W. Wang, S. Zhang, M.-A. Bisotti, M. Franchin, C.L. Hu, R. Stamps, T. Hesjedal, H. Fangohr, Proposal of a micromagnetic standard problem for ferromagnetic resonance simulations, J. Magn. Magn. Mater. 421 (2017) 428–439, https://doi.org/10.1016/j.jmmm.2016.08.009.

[34] M.-W. Yoo, J. Lee, S.-K. Kim, Radial-spin-wave-mode-assisted vortex-core magnetization reversals, Appl. Phys. Lett. 100 (17) (2012) 172413, , https://doi.org/10.1063/1.4705690.

[35] Z. Wang, M. Li, R. Wang, Resonance beyond frequency-matching: multidimensional resonance, New J. Phys. 19 (3) (2017) 033012, , https://doi.org/10.1088/1367-2630/aa6275.

[36] B.W. Zingsem, M. Farle, R.L. Stamps, R.E. Camley, Unusual nature of confined modes in a chiral system: Directional transport in standing waves, Phys. Rev. B 99 (2019) 214429, , https://doi.org/10.1103/PhysRevB.99.214429.

[37] K.Y. Guslienko, W. Scholz, R.W. Chantrell, V. Novosad, Vortex-state oscillations in soft magnetic cylindrical dots, Phys. Rev. B 71 (2005) 144407, , https://doi.org/10.1103/PhysRevB.71.144407.

[38] H. Zhang, Y. Liu, M. Yan, R. Hertel, Azimuthal spin wave modes excited in an elliptical nanomagnet with vortex pair states, IEEE Trans. Magn. 46 (6) (2010) 1675–1678.

[39] M.-W. Yoo, S.-K. Kim, Azimuthal-spin-wave-mode-driven vortex-core reversals, J. Appl. Phys. 117 (2) (2015) 023904, , https://doi.org/10.1063/1.4905689.